ELSEVIER

Contents lists available at ScienceDirect

Sensors and Actuators: B. Chemical

journal homepage: www.elsevier.com/locate/snb





Low-cost rapid prototyping for microfluidics using Parafilm®-based microchannels for low resource settings

Zhenglong Li ^a, Niranjan Haridas ^a, Sreerag Kaaliveetil ^a, Yu-Hsuan Cheng ^a, Charmi Chande ^a, Veronica Perez ^b, Amir K. Miri ^b, Sagnik Basuray ^{a,b,*}

- ^a Department of Chemical and Materials Engineering, New Jersey Institute of Technology, Newark, NJ 07102, United States
- b Department of Biomedical Engineering, New Jersey Institute of Technology, Newark, NJ 07102, United States

ARTICLE INFO

Keywords:
Parafilm® sheet
Plotter cutter
Microfluidic electrochemical transducer
Three-dimensional microfluidics

ABSTRACT

We presented a novel strategy of using Parafilm® sheets for making microchannels in rigid substrates-based microfluidic devices with fast prototyping and cost-effectiveness. The strategy uses a Plotter cutter and Parafilm® sheets via the Thermal fusing bonding method to prepare Rigid substrate-based Microfluidics (PPTR μ) in a short span of ~ 10 min. The Cricut® Explore plotter cutter, as a cheaper alternative to conventional laser cutters, with a $\sim 500~\mu m$ resolution to Parafilm® sheet, was shown to create sharp angle micropatterns with a uniform angular distribution. Process parameters like sealing temperature were optimized to minimize channel deformation and enhance device sealing. A 55 °C sealing temperature shows sufficient bonding strength and ensures minimal microchannel width deformation (< 5%). Parafilm® sheets used to make the microchannels showed good chemical resistance to different pH and polar solvent environments. The practical use of the PPTR μ protocol to prepare a two-dimensional concentration gradient generator and a microfluidic electrochemical transducer was successfully demonstrated. The same protocol was extended by appropriately extending the sealing time to 10 min to prepare a three-dimensional microfluidic device with a hybrid structure of "glass-Parafilm®-glass-Parafilm®-glass."

1. Introduction

Thousands of novel microfluidic point-of-care (PoC) diagnostic platforms and applications have been published over the past two decades [1]. Polydimethylsiloxane (PDMS) has been widely used in microfluidics due to its excellent biocompatibility, high optical transparency, and ease of fabrication (Table 1). However, fabricating microfluidic channels using PDMS usually involves costly and laboratory-intensive etching, baking, or bonding steps in cleanroom environments. To simplify fabrication and lower costs, microchannels have been fabricated using thermoplastics such as Polymethyl methacrylate (PMMA) and Adhesive double-sided tapes (ADST) [2-4]. PMMA layer-by-layer chips are widely used in microfluidic applications due to their low cost and high optical transparency [5]. However, PMMA-based microfluidics has a significant drawback in meeting fast prototyping needs. ADSTs like ARcare® 90106NB and ARseal™ 90880 are popular for the scalable production of microchannel layers in microfluidics [3,6, 7]. However, the adhesive residuals and high-cost limit their use in microfluidic chips. For example, for the double-sided tape (ARcare\$ 90106NB), one roll of 0.75 feet x 30 feet (in width x length, respectively) will cost around \$300.

Parafilm® sheet is a low-cost, stretchable, sticky thermoplastic material extensively used in laboratories for sealing or protecting vessels. Parafilm® sheet is composed of polyolefin and wax, melting at around 60 °C. Parafilm® is increasingly used to build sidewalls of microchannels in microfluidic paper-based analytical devices (μ PADs) [4, 13–15]. For example, Koesdjojo et al. demonstrated a colorimetric microfluidic device using Parafilm® infused paper to detect heavy metal ion substrates [13]. In another recent work reported by Kim et al., a three-dimensional (3D) push-on valve is demonstrated using Parafilm® infused paper [14]. The use of Parafilm® in μ PADs is because the melted Parafilm® wax penetrates paper's cellulose fibers at high pressure and temperature, solidifying as the temperature drops, creating hydrophobic barriers in the paper networks. However, the use of Parafilm® to prepare microchannels in μ PADs also faces some drawbacks, such as the deformation of microchannel dimensions, mainly due to the

^{*} Corresponding author at: Department of Chemical and Materials Engineering, New Jersey Institute of Technology, Newark, NJ 07102, United States. E-mail address: sbasuray@njit.edu (S. Basuray).

Table 1 A summary of different microfluidic chip materials [8–12].

Materials	Advantage	Disadvantage	Microchannel Preparation	Bonding Strategy
PDMS	Bio-compatible; Easy-to-mold; Gas permeable; Low autofluorescence	Water permeability; Swelling in organic solvents; Incompatible with large-scale manufacturing; Adsorption of hydrophobic molecules	Soft lithography	Plasma treatment
PMMA	Bio-compatible; High Scratch resistance; Environmental sustainability; Recyclable	Incompatible with fast prototyping; Limited heat resistance (80 °C); Limited chemical resistance	Injection molding; Hot embossing; Laser ablation; Reactive ion etching	Thermal bonding, Solvent bonding, Adhesive bonding
ADST	Compatible with fast-prototyping; Low auto- fluorescence; Excellent flexibility	Poor optical qualities; Inherent resolution limitations; Difficult to make multilayer architecture; Residuals from adhesive materials	Laser ablation; Xurography;	Adhesive bonding

heat-assisted lamination process and the inhomogeneity of the porous paper structure [15]. Laser ablation and plotter cutting are two simple and popular methods for cutting microfluidic channels in thermoplastics. Both methods have a similar workflow: a laser or knife feeds and cuts the substrate. Laser cutters have the advantage of non-contact cutting and higher resolution. However, these benefits come at the expense of high equipment costs [16]. Plotter cutting, or xurography, uses a drag knife printer to cut microfluidic designs from laminate substrates. While these methods do not provide the superior resolution of photolithography methods, their use is more translatable to scalable manufacturing methods [3].

Inspired by these interesting previous works and based on the principle of "do-it-yourself," cost-effectiveness, and rapid prototyping. We propose a novel method of using a plotter cutter and Parafilm® sheets via the thermal fusing bonding method to prepare rigid substrate-based microfluidics (PPTR μ) for the first time. Here, silica glass slides are adopted as substrates of microfluidic devices. This is because rigid substrates are more economical, easy to assemble, and reliable than flexible substrates for creating miniaturized microfluidic electrochemical transducers (μ FETs) [17–20]. Silica glass slides are still one of the most used rigid substrates to perform various microelectrode (μ E) layers or dielectric depositions [21,22]. The Parafilm® sheets are adopted to prepare microchannel patterns and used as middle bonding layers in the hybrid "glass + Parafilm® + glass" systems. During the thermal fusion process, a static pressure of 2.5 kPa is applied to remove air bubbles between the layers of the hybrid device system.

As a proof-of-concept, practical adoption of the proposed PPTR μ strategy to prepare two-dimensional (2D) concentration gradient generators (CGG), μ FETs, and 3D microfluidics have been carried out. The temperature's influence on the device sealing is studied, and it is found that a 55 °C sealing temperature shows sufficient bonding strength (\sim 0.13 MPa) while ensuring minimal deformation (< 5%) of the Parafilm® microchannel geometry. Silica glasses are chosen as the substrates here, while any rigid substrates, including silicon and hard plastic substrates, can be used. This proposed fast prototyping, cost-effectiveness, and easy-to-adopt PPTR μ protocol can be an ideal alternative for preparing

robust microfluidic devices for other research groups.

2. Experimental section

2.1. Chemicals and equipment

Potassium nitrate (KNO₃), 99%, was purchased from Thermo Fisher Scientific. Potassium Ferri/ferrocyanide (K₃/K₄[Fe(CN)₆]) (99.0% min Crystalline) was purchased from Sigma-Aldrich. Commercially available water-soluble food colorings were purchased from Modern Biology Inc. for the microchannel characterizations. Isopropyl alcohol (99%, ASC) was purchased from VWR Chemicals BDH® and used for cleaning the glass slides. Different solvents, including Acetone (≥ 99.5%, VWR Chemicals BDH®), Dimethyl Sulfoxide (DMSO, ≥ 99.7%, Sigma-Aldrich), Methanol (VWR Chemicals BDH®), Ethanol (94-96%, Alfa Aesar), and N, N-Dimethylformamide (DMF, anhydrous, 99.8%, Sigma-Aldrich), were used for different solvent-resistant testing for the Parafilm® channel. The super glue was brought from the LOCTITE®. The deionized (DI) water was collected from a Milli-Q® Direct 8 Water Purification System and, without further purification, was used to prepare coloring solutions and target analytes needed in the experiments. Super glue from Loctite® was used to glue the tube connector to the prepared devices. The electrical conductivity meter was purchased from HORIBA. Parafilm® wrapping sheet was ordered from Thermo Fisher Scientific. Adhesive double-sided tapes (ARseal™ 90880 and ARcare® 90106NB) were purchased from Adhesive Research®. Standard glass slides with a dimension of 75 mm \times 25 mm x 1 mm in height x width x length were purchased from Globe Scientific Incorporated and used as substrates for microfluidic devices or electrode deposition. A drill press ordered from central machinery was used to prepare ports for the microfluidic chips. The interfacial bonding strength between the Parafilm® layer and glass substrates was tested using a tensile tester obtained from Instron® (Serial Number: VS04180724). The channel characterization of assembled devices was conducted using a Scanning Electron Microscope (SEM, Model: JSM-7900 F SEM) and an optical microscope (Olympus BX51). The NE-300 syringe pump from New Era Pump Systems, Inc. (USA) was used to pump the target solutions through the studied devices.

2.2. Parafilm® sheets based device preparation

Parafilm® sheet was used here as the channel and middle bonding layer (Fig. S1). A Cricut® Explore machine (No: CXPL0001) was first used to get pre-designed micropatterns in the Parafilm® sheets. The Parafilm® sheet with micropatterns was transferred from the cutting mat (12 in x 12 in) to the glass substrates and thoroughly cleaned using Acetone. The top glass slides were drilled with the inlet and outlet holes. This work used a non-automated drill press with a drill bit diameter of 0.5 mm to create inlet and outlet holes. Unlike the automated one, which is more applicable to delicate patterns, this relatively cheap, nonautomated drill press makes it more available to people who want to DIY alone. The assembled device was then placed onto a hot plate and applied with a static pressure of around 2.5 kPa for about 5 min. The superglue bonds the tube connector to the inlet and outlet holes. The food coloring or target analyte solutions were passed through the microchannel using New Era pumps. The total fabrication time was less than 10 min, which makes it attractively easy to design and fabricate versatile structures with this simple PPTRµ protocol.

3. Results and discussion

3.1. Comparison of plotter-cut thermoplastics

Creating micropatterns with sharp angles is still challenging during preparation [23–25]. The applicability of the plotter cutter to design micropatterns with sharp angles in the soft thermoplastic Parafilm® was tested. Two widely-used double-sided tapes, including ARsealTM 90880



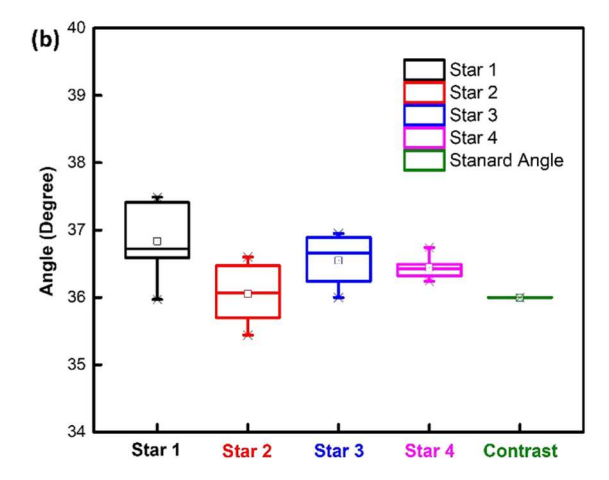


Fig. 1. (a) Image of Parafilm® sheet that cut with star-shaped patterns. (c) Box plot statical results of the angular values of the star-shaped patterns.

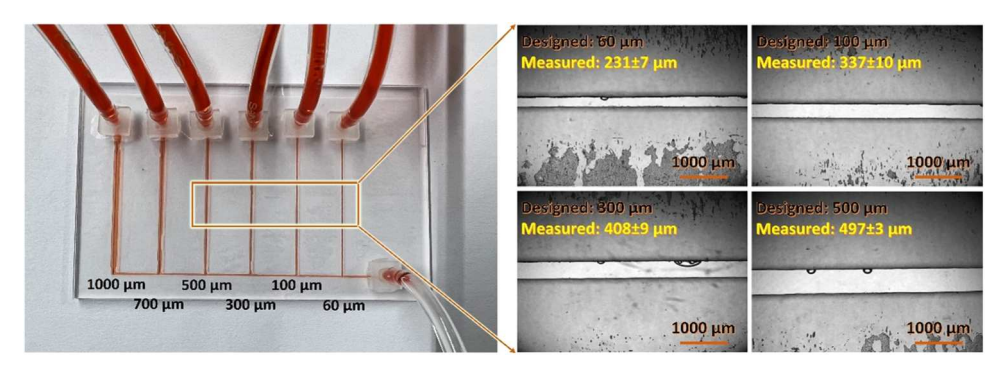


Fig. 2. (Left) Picture of a proof-of-concept device with multiple microfluidic channels of different widths. (Right) Optical microscope images of selected microchannels.

(thickness = $\sim 140~\mu m)$ and ARcare® 90106NB (thickness = $\sim 140~\mu m)$, were compared with the Parafilm® sheet (at a similar thickness of around 130 μm). Fig. S2 shows that the plotter cutter failed to get the

designed micropatterns in the two double-sided tapes. It was surprisingly easy to get these sharp micropatterns in Parafilm® sheet since it has a softer texture than the other two thermoplastic double-sided tapes.

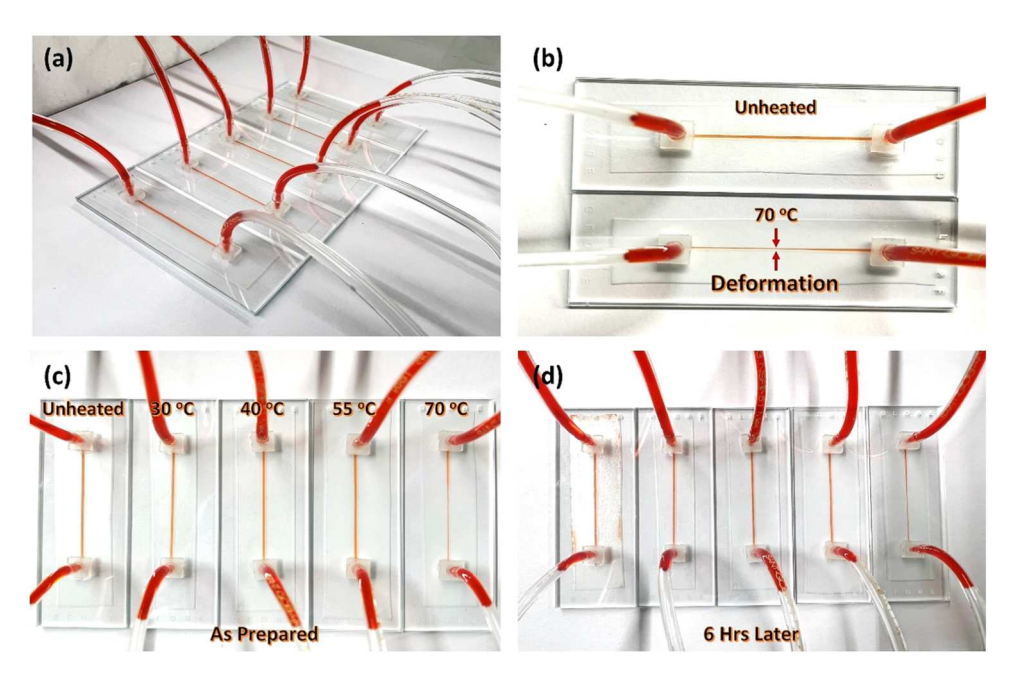


Fig. 3. (a) A picture of microfluidic devices prepared under different combinations of temperatures (room temperature, 35 °C, 45 °C, 55 °C, and 70 °C). (b) A comparison of microfluidic devices prepared under room temperature and 70 °C. (c) and (d) Comparison of microfluidic devices prepared under different temperatures and time points.

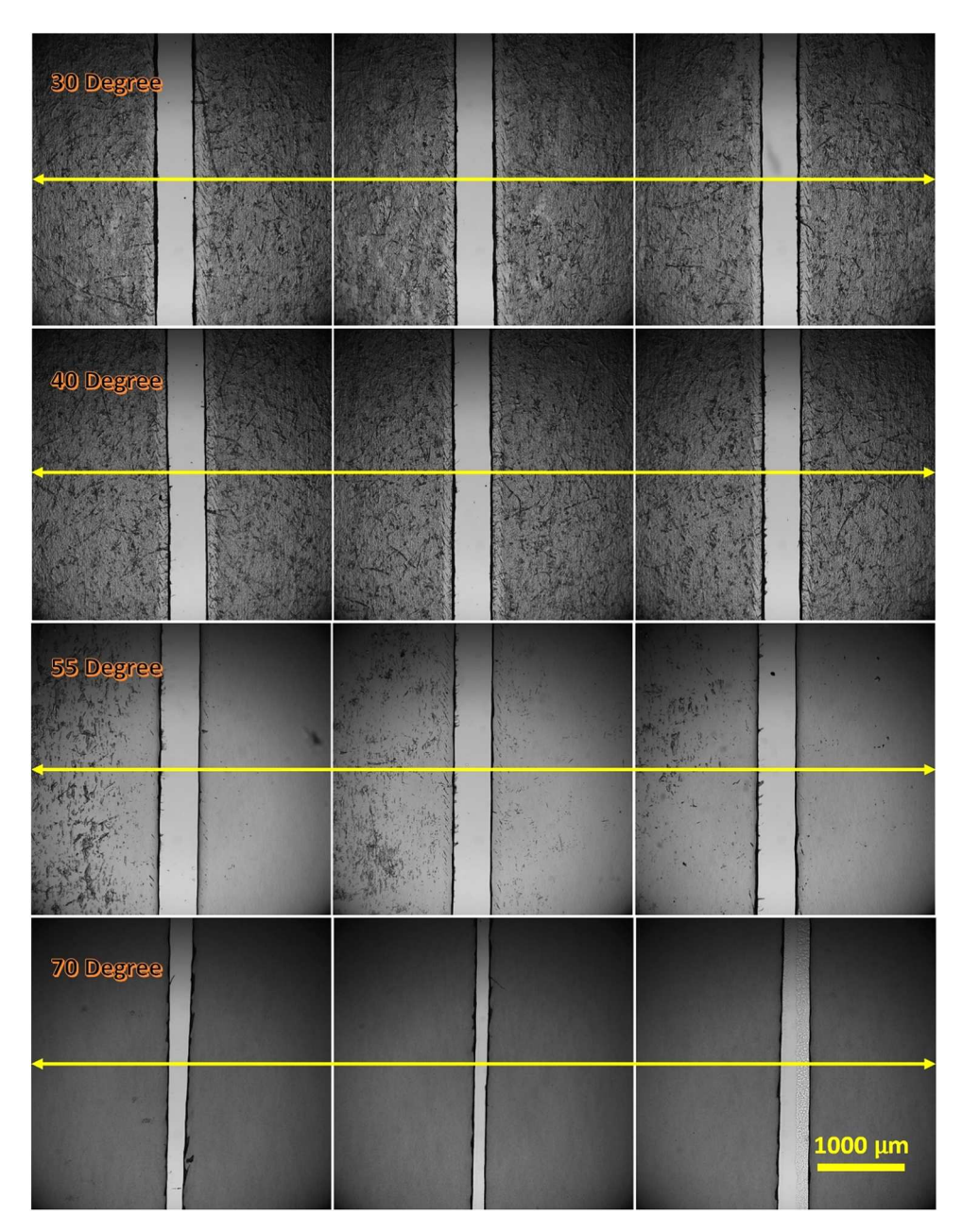


Fig. 4. Optical images of microchannels prepared under different sealing temperatures. From top to bottom, the sealing temperature is 30 °C, 40 °C, 55 °C, and 70 °C, respectively. The length of the scale bar is 1000 μ m, which applies to all images shown in Fig. 4.

Therefore, compared to the ARsealTM 90880 and ARcare® 90106NB double-sided tapes, a plotter cutter is more reliable to prepare microchannels in soft plastics, such as Parafilm® sheet. Fig. 1 shows the adoption of a plotter cutter to compose classical star-shaped sharp-angle micropatterns in the Parafilm® sheet. The five sharp angles of each pattern are calculated via the software ImageJ (NIH) and presented in Fig. 1(b). The statistical results show that the created micropatterns have a uniform angular distribution. However, the technical limitations of the blade rotation at the endpoint will result in the deformation of the patterns (Fig. S3). A plotter cutter makes preparing Parafilm microchannels in Parafilm® more efficient and easier, especially for microchannels that do not have complicated designs.

3.2. Resolution study of Cricut® explore plotter cutter

Instead of using a laser cutter with a spot size of tens of micrometers, in this present work, we opted for a plotter cutter to prepare micro-

channels in Parafilm® sheet, which is more suitable for mass manufacturing and rapid prototyping [14,15,26]. The channel size is essential for microfluidics, as it can directly determine the amount of sample and reagents required to perform the assay [27]. The channel size can directly affect a microfluidic sensor's sensitivity and selectivity [28]. Therefore, for the Cricut® Explore plotter cutter used in this work, it is necessary to confirm its resolution when used for the Parafilm® sheet. The resolution is defined as the minimum cutting size with a discrepancy (Δ_D , Eq. (1)) less than 5% [29].

$$\Delta_D = \left| \frac{V_{design} - V_{device}}{V_{design}} \right| * 100\% \tag{1}$$

Where $V_{\rm design}$ represents the designed channel width and $V_{\rm device}$ is the measured prepared device width.

One device with multiple microchannels was prepared for this measurement, as shown in Fig. 2. From left to right, the microchannels have different designed channel widths of 1000, 700, 500, 300, 100, and

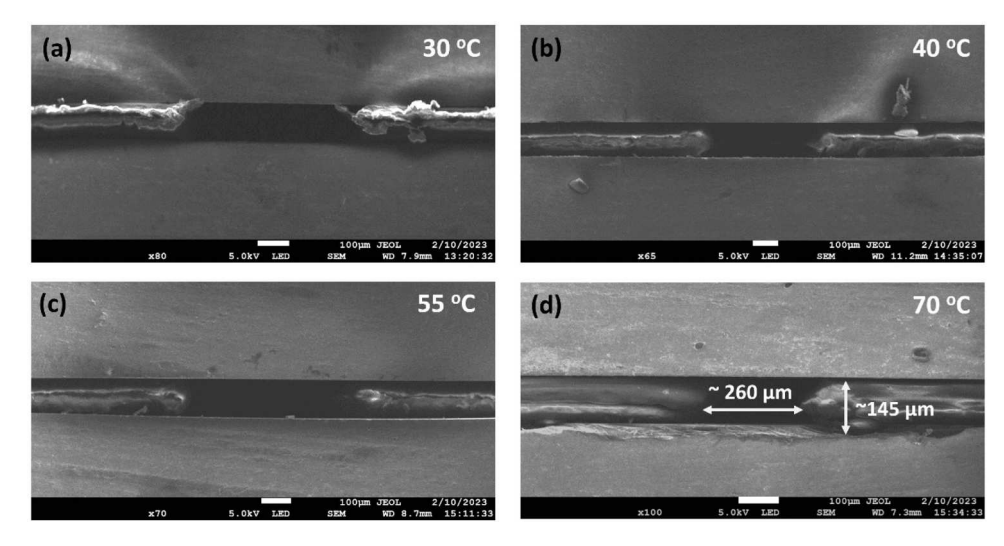


Fig. 5. Cross-section SEM image of Parafilm® microchannel that is prepared under (a) 30 °C, (b) 40 °C, (c) 55 °C, and (d) 70 °C sealing temperature.

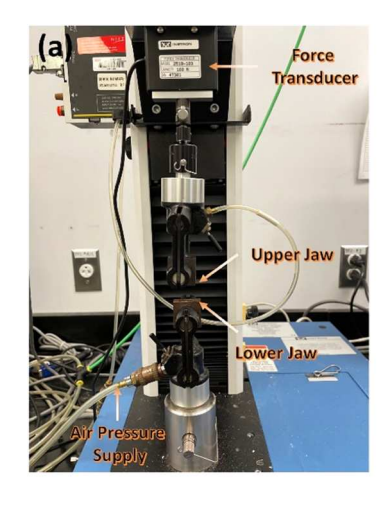
60 µm, respectively. From the microscopy images, it was found that the actual measured channel width for 500 µm is 497 \pm 3 µm, for 300 µm is 408 \pm 9 µm, for 100 µm is 337 \pm 10 µm, and for 60 µm is 231 \pm 7 µm, respectively. A considerable Δ_D in the channel width happens when the designed cutting dimension is reduced below 300 µm. Based on Eq. (1), a Δ_D of \sim 36%, \sim 1370%, and \sim 2850% is observed for the designed channel of 300, 100, and 60 µm, respectively. A sharp increase in the cutting discrepancy appears when the channel width is reduced to 100 µm; however, a Δ_D of only \sim 1% is observed for the 500 µm designed channel. We observed that the resolution of the Cricut® Explore plotter cutter is about 500 µm, i.e., the smallest size that can be cut within an acceptable margin of Δ_D .

3.3. Influence of temperature on device sealing

Parafilm® is a thermoplastic material whose properties are greatly influenced by temperature [30,31]. To ensure sufficient bonding strength and prevent leakage while maintaining the pre-designed microchannels, the study of temperature's influence on device sealing is presented in Fig. 3. A microchannel with a dimension of 40 mm \times 500 μm x 130 μm in length x width x height was cut in the Parafilm® sheet and used in the prepared proof-of-concept devices (Fig. 3(a)). Five microfluidic devices were designed using silica substrates under different sealing temperatures, ranging from room temperature to 70 °C. Static pressure of approximately 2.5 kPa was applied

for about 5 min to each device. The devices prepared under different temperatures were subsequently characterized by pumping red food coloring with a flow rate of 1 ml/min. Fig. 3(b) displays the device prepared at 70 °C with a visible microchannel distortion. Figs. 3(c) and 3(d) compare prepared microchannels at different points in time. Fig. 3 (d) shows that the adhesive force between the glass slides and Parafilm® sheet layer cannot prevent leakage at room temperature.

The images in Fig. 4 were taken before passing the red coloring, from left to right, were taken at a 1 cm distance from the top end of the channel (Fig. 3(c)), the middle of the channel, and 1 cm from the end of the channel, respectively. The channel width along the yellow double arrow solid line was collected and analyzed for each temperature condition. An analysis of the variations in the channel width is shown in Fig. S4(a). For the microchannels prepared under 70 °C sealing temperature, the discrepancy between the $V_{\rm design}$ and $V_{\rm device}$ rises to \sim 65.3% at 70 °C. For other cases, this value is lower than 5%. In addition, upon careful comparison of the images, we observed that the contacted areas between the Parafilm® sheet layer and glass slides became more transparent as the sealing temperature increased. Removing the tiny air bubbles from the hybrid sandwiched structure of "glass-Parafilm®-glass" can help the transparency. The existence of air bubbles is one of the main reasons for the leakage [32,33]. Additionally, the variations in channel thickness were examined along with changes in width (Fig. 5). The microchannels prepared under 55 °C sealing temperature have a similar channel thickness of around 130 µm, the thickness of a pristine



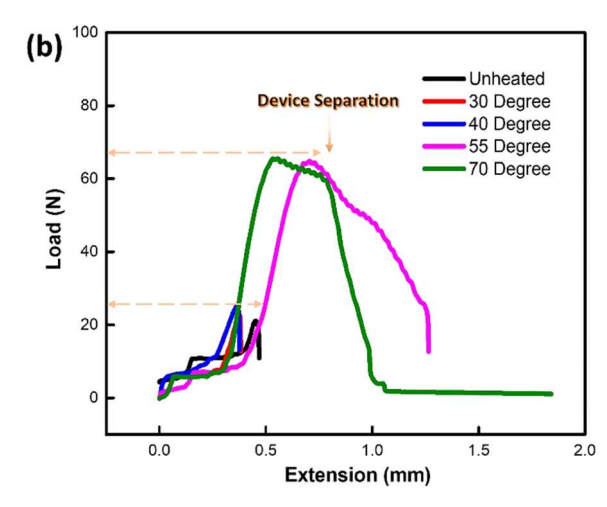


Fig. 6. (a) Setup of the tensile strength test. (b) Bonding strength of different device samples that are prepared under different sealing temperatures.

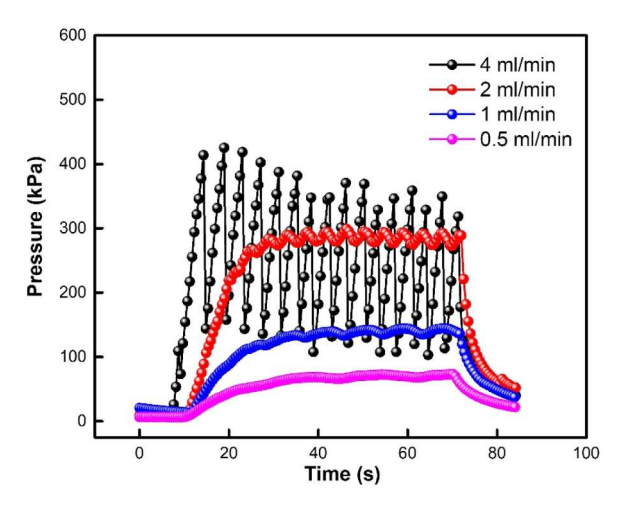


Fig. 7. The relationship between different flow rates and inlet pressures.

Parafilm® sheet [29]. While for the 70 °C case, the thickness of the Parafilm® microchannel is increased to $\sim 145~\mu m$. Therefore, the Parafilm® sheet cannot keep its initial geometric structure when packaged at high temperatures ($\geq 70~^{\circ}$ C).

The interfacial adhesion property is tested using a tensile tester (Fig. 6(a)). Here, the device samples were firmly held by the upper and lower jaws, prepared under different sealing temperatures, and with the same contact area of $\sim 500~\text{mm}^2$ (Fig. S5). During the testing, the upper jaw moved upward at a uniform speed of 15 mm/min, and the tensile force was recorded simultaneously until the glass slides failed to bond. Corresponding results are shown in Fig. 6(b). The results obtained show that compared to the devices prepared with 30 °C and 40 °C sealing temperatures, the devices prepared at sealing temperatures of 55 °C and 70 °C have a much higher bonding strength ($\sim 0.13~\text{MPa}$) as shown in Fig. S4(b). During testing, it was observed that the glass slides broke before separating from the Parafilm® sheet at temperatures $\geq 55~\text{°C}$. It has been found that a sealing temperature of 55 °C can both prevent geometric deformation of the microchannels and ensure strong bonding.

As shown in Fig. 7, the inlet pressures were measured under different flow rates (0.5, 1, 2, 4 ml/min). Fig. S6 shows the complete testing system. As shown in Fig. S7, there was no observed leakage at the highest flow rate of 4 ml/min (pump limitation), and the inlet pressure was approximately 0.4 MPa. The observed pressure profile fluctuations

are related to the pumping pulses from the pump. Similarly, for the cases of 2, 1, and 0.5 ml/min, the inlet pressure is around 0.3, 0.13, and 0.07 MPa, respectively. These results demonstrate that a sealing temperature of 55 $^{\circ}\text{C}$ is sufficient to prevent potential device leakage when the inlet pressure is less than 0.4 MPa. Unless otherwise stated, the devices below are set with a sealing temperature of 55 $^{\circ}\text{C}$.

3.4. Practical application of PPTRµ to prepare 2D CGG and µFET

As shown in Fig. 8, the use of Parafilm® microchannel with a designed channel width of 500 μm in a 2D concentration gradient generator (CGG) and microfluidic electrochemical transducer, μFET , is demonstrated. A 2D CGG is prepared based on the proposed PPTR μ protocol, and no leakage is observed. Here, 100 mM KNO $_3$ and 50 mM K $_{3/4}$ [Fe(CN) $_6$] in 100 mM KNO $_3$ were pumped into the CGG with a 100 $\mu L/min$ flow rate. Solution samples from different reservoirs were collected and tested to verify whether a concentration gradient was successfully created. Therefore, a μFET made by two pairs of non-planar interdigitated μEs (hereafter, NP- μFET) and using one middle Parafilm® microchannel/bonding layer was prepared for the subsequent verification.

The collected cyclic voltammograms (CV) from the NP-µFET using different solution samples are demonstrated in Fig. 9(a). The voltammogram of 50 mM $K_3[Fe(CN)_6]$ and $K_4[Fe(CN)_6]$ (1:1, mole ratio) in KNO3 (100 mM) at a scan rate (v) of 100 mV/s shows oxidation at anodic peak potential (E_{pa}) of ~ 110 mV Pt RE and a back reduction at cathodic peak potential (E_{pc}) at ~ -80 mV vs. Pt RE. Similarly, corresponding values are summarized in Table 2 for other solutions collected from the reservoirs. The gradual decrease (from Reservoir 4 to Reservoir 1) in the current density (the cathodic and anodic processes' peak currents $(I_{pc}/I_{pa}))$ demonstrates that a concentration gradient of the [Fe (CN)₆]^{3-/4-} redox couple has been generated in the collected solutions samples. Furthermore, the collected differential pulse voltammograms (DPV) and electrochemical impedance spectroscopy (EIS) from NP-µFET using different solution samples are demonstrated in Fig. 9(b) and 9(c), respectively. For the DPV results, a typical voltammogram of the 50 mM [Fe(CN)₆]^{3-/4-} couple appears at a peak potential (E_{peak}) of ca. 5 mV and with a full width at half maximum (FWHM) of ~ 120 mV. E_{peak} @ 5 mV, 7 mV, 7 mV, and 2 mV can be observed for the solutions obtained from Reservoir 4, 3, 2, and 1, respectively. An FWHM of 120 mV, 117 mV, 108 mV, and 114 mV are observed for the solutions obtained from Reservoirs 4, 3, 2, and 1, respectively. Similarly, like in the CV test, a

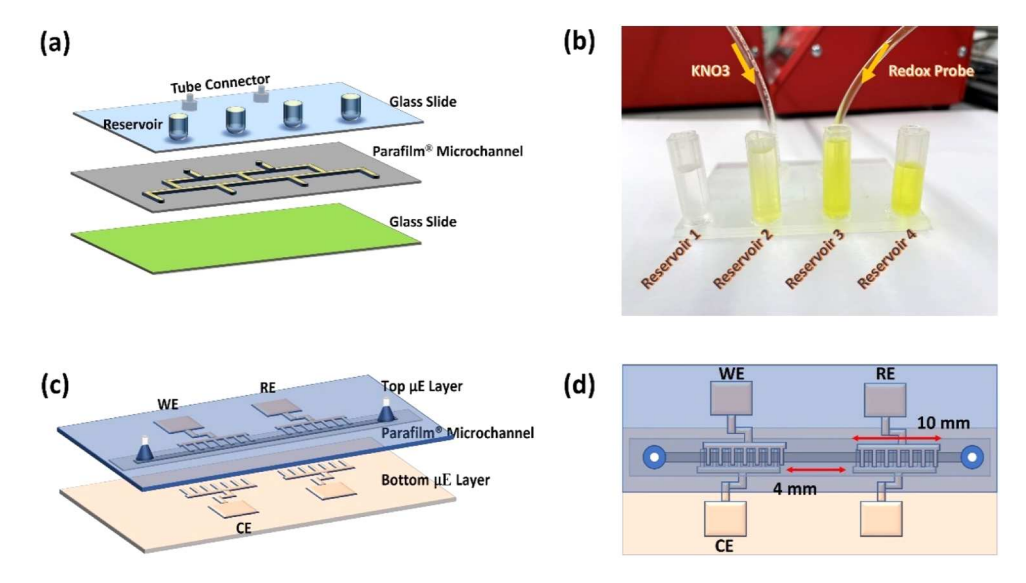


Fig. 8. (a) Schematic diagram and (b) a picture of 2D concentration gradient generator. (c) Side-view and (d) Top-view of a fully integrated non-planar interdigitated microelectrodes based μFET (NP-μFET).

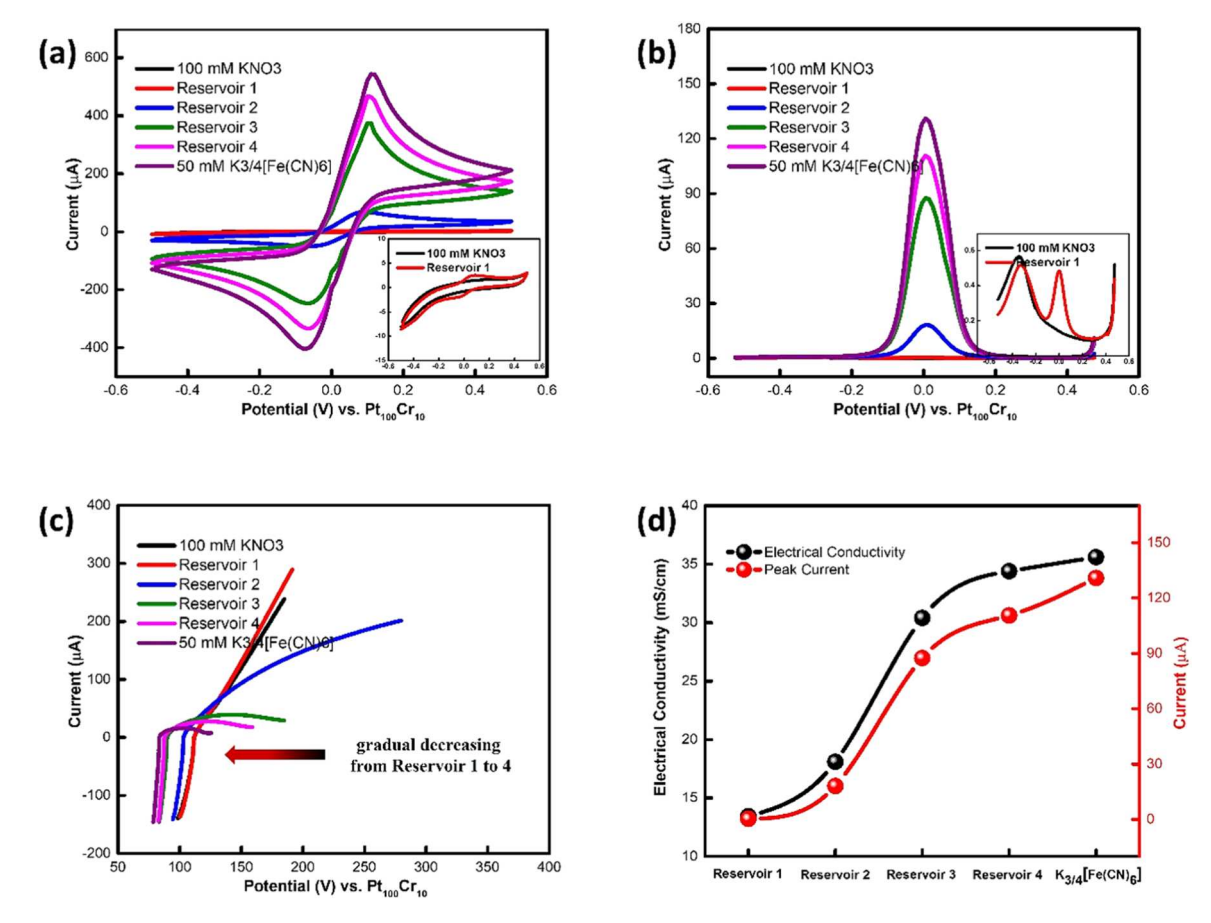


Fig. 9. (a) Cyclic voltammograms, (b) Differential pulse voltammograms, and (c) Electrochemical impedance spectroscopy that are obtained from NP- μ FET using different solutions, including 100 mM KNO₃, 50 mM K_{3/4}[Fe(CN)₆], and solutions collected from different reservoirs. (d) Electrical conductivity testing results and corresponding DPV peak current results from different solutions, including 100 mM KNO₃, 50 mM K_{3/4}[Fe(CN)₆], and solutions collected from different reservoirs.

Table 2 Redox Features of Fe(CN) $_{6}$ J $^{3-/4-}$ Couple in NP- μ FET.

Solutions	E _{pa} (mV)	I _{pa} (μA)	E _{pc} (mV)	I _{pc} (μA)
50 Mm K _{3/4} [Fe(CN) ₆]	~ 110	~ 605	~ - 80	~ 507
Reservoir 4	~ 103	~ 515	~ - 64	~ 423
Reservoir 3	~ 105	~ 405	~ - 68	~ 309
Reservoir 2	~ 92	~ 73	~ - 64	~ 59
Reservoir 1	~ 85	~ 1.5	~ -58	~ 1.1

gradual decrease (from Reservoir 4 to Reservoir 1) in the peak currents that related to the $[Fe(CN)_6]^{3-/4}$ - couple's reduction process is observed (Fig. 9(d)). More details about the electrical conductivity can be found in Table S1. The EIS results in Fig. 9(c) also clearly show us that the value of the intersection of the EIS curve with the x-axis (representing the resistance of the solution trapped between the top and bottom μE layers) decreases as the solution changes from Reservoir 1 to Reservoir 4. This is because the solution concentration between the top and bottom μE layers increases from Reservoir 1 to Reservoir 4. Therefore, all the results demonstrate the successful practical use of Parafilm® sheet to prepare 2D CGG in silica rigid substrates-based microfluidic chips.

3.5. Chemical resistance of Parafilm® channel

Parafilm® channel was tested for its chemical resistance to acid/base and organic polar solvents in challenging practical use. Fig. S8 illustrates a proof-of-concept device that consists of three identical microchannels. After sealing, three different coloring solutions with varied pH values (4 to 10) were pumped through the microchannels to examine the flow

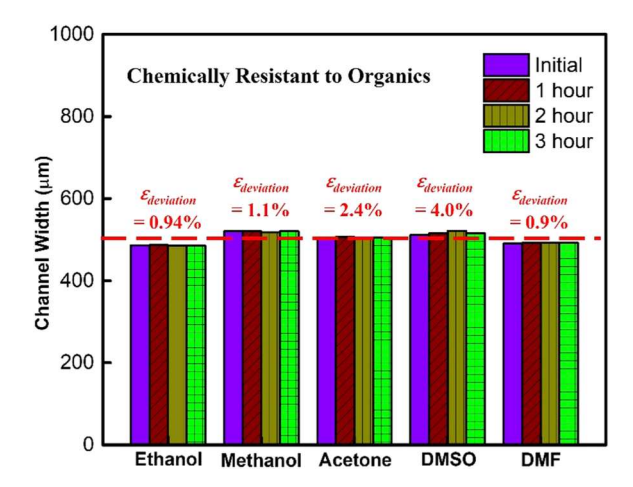


Fig. 10. Statistical results of the channel width variation along the running of different solvents. The height of the red dotted line is $500~\mu m$.

profile. The microscope images showed no noticeable changes in the channel's shape or size. The study suggests that Parafilm® sheets exhibit strong chemical resistance across various pH environments. Furthermore, five assembled microfluidic devices with identical 500 μm width were prepared for testing organic polar solvents (Fig. S9). The relevant statistical results are shown in Fig. 10. During the observation period (three hours), the channel width remained constant with negligible variations ($\epsilon_{deviation} < 5\%$). After the observation, no leakage was observed.

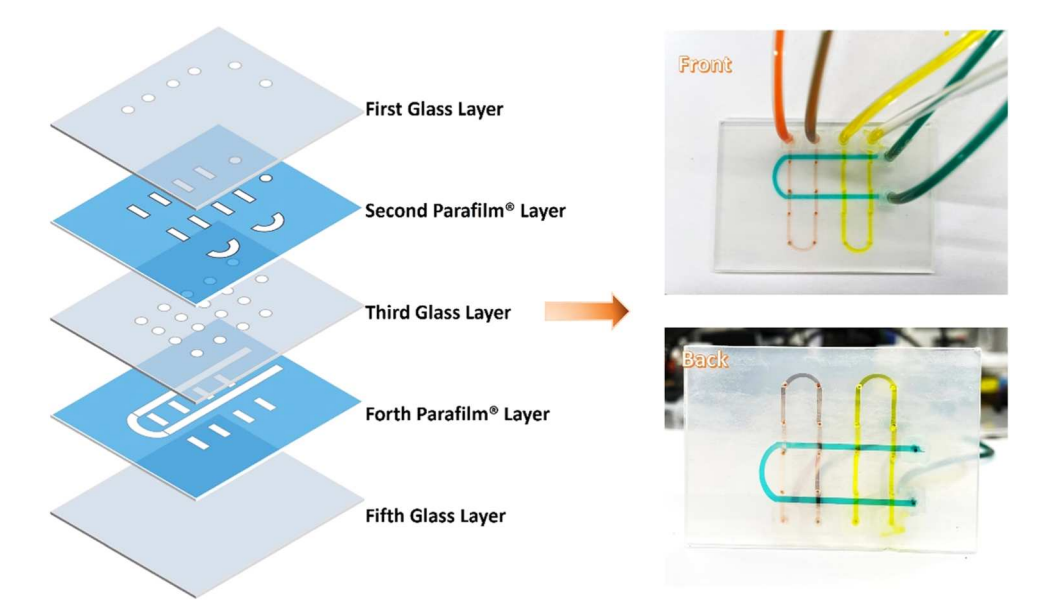


Fig. 11. (Left) Side-view of 3D microfluidics made by Parafilm microchannel/bonding sheets. (Right) A picture of the prepared 3D microfluidics.

3.6. Extension of PPTRµ protocol to prepare 3D microfluidics

3D microfluidic devices have a higher density of functional structures (e.g., movable membranes and porous mats) than their 2D counterparts, which allows for complex fluid manipulation and multiple analytical tests [34]. The traditional way of using PDMS is challenging for building complex 3D structures because the bonding of PDMS usually requires silane coupling agents to treat the PDMS surface [29]. The device is generally created by sequentially bonding one layer at a time. To extend the application of the proposed PPTR μ sealing protocol, 3D microfluidic devices with a hybrid structure of "glass-Parafilm®-glass/Parafilm®-Parafilm®-glass" were tried here, as shown in Fig. 11 and S10. For adequate bonding, the thermal bonding time for the 3D microfluidic device in Fig. 11 is extended from 5 to 10 min. Here, three different coloring solutions are pumped through the device with a 100 μ L/min flow rate, and no leakage was observed during the flow characterization.

4. Conclusion

This work has demonstrated the feasibility of using a Plotter cutter and Parafilm® sheets via the Thermal fusing bonding method to prepare Rigid substrates-based Microfluidics (PPTRµ). The study has confirmed the practicality of using a cheap plotter cutter (Cricut® Explore) to create micropatterns in Parafilm® sheets with high precision. We studied the effect of processing temperature on bond strength, channel deformation, and device sealing. We found that a sealing temperature of 55 °C is sufficient for achieving strong bonding (~ 0.13 MPa) while minimizing channel deformation, with a discrepancy in the microchannel width of less than 5.0%. This study demonstrates that the PPTRµ protocol simplifies the preparation of microfluidic devices, including a two-dimensional concentration gradient generator and a microfluidic electrochemical transducer, which were successfully characterized. The extension of our protocol to prepare a three-dimensional microfluidic device with a hybrid structure of "glass-Parafilm®-glass-Parafilm®glass" has also been proved by appropriately extending the sealing time from the previous 5 min to 10 min. The current protocol presents a fast, cost-effective, and easily adaptable approach for constructing robust and sophisticated microfluidic devices for various research applications.

CRediT authorship contribution statement

Zhenglong Li, and Veronica Perez performed Experiments, Writing – original and revised drafts, and Conceptualization. Niranjan Haridas, Sreerag Kaaliveetil, Yu-Hsuan Cheng, and Charmi Chand performed Writing and Editing. Sagnik Basuray and Amir Miri performed Writing – review and editing, and Conceptualization.

Declaration of Competing Interest

The authors declare that they have no known competing financial interests or personal relationships that could have appeared to influence the work reported in this paper.

Data Availability

Data will be made available on request.

Acknowledgments

This manuscript is supported by Sagnik Basuray's NSF grant # 1751759, Career: "ASSURED" electrochemical platform for multiplexed detection of Cancer Biomarker Panel using Shear Enhanced Nanoporous Capacitive Electrodes. A.K.M. acknowledges the financial support from NIH (R21-DC018818).

Appendix A. Supporting information

Supplementary data associated with this article can be found in the online version at doi:10.1016/j.snb.2023.135212.

References

- G.M. Whitesides, The origins and the future of microfluidics, Nature 442 (2006) 368–373.
- [2] D. Patko, Z. Mártonfalvi, B. Kovacs, F. Vonderviszt, M. Kellermayer, R. Horvath, Microfluidic channels laser-cut in thin double-sided tapes: Cost-effective biocompatible fluidics in minutes from design to final integration with optical biochips, Sens. Actuators B: Chem. 196 (2014) 352–356.
- [3] P. Khashayar, G. Amoabediny, B. Larijani, M. Hosseini, S. Van Put, R. Verplancke, et al., Rapid prototyping of microfluidic chips using laser-cut double-sided tape for electrochemical biosensors, J. Braz. Soc. Mech. Sci. Eng. 39 (2017) 1469–1477.
- [4] S.H.S. Tali, H. Hajimiri, Z. Sadiq, S. Jahanshahi-Anbuhi, Engineered detection zone to enhance color uniformity on paper microfluidics fabricated via Parafilm®heating-laser-cutting, Sens. Actuators B: Chem. (2023) 133324.

- [5] X. Chen, J. Shen, M. Zhou, Rapid fabrication of a four-layer PMMA-based microfluidic chip using CO₂-laser micromachining and thermal bonding, J. Micromech. Microeng. 26 (2016) 107001.
- [6] P. Gu, K. Liu, H. Chen, T. Nishida, Z.H. Fan, Chemical-assisted bonding of thermoplastics/elastomer for fabricating microfluidic valves, Anal. Chem. 83 (2011) 446–452.
- [7] Z. Li, Y.-H. Cheng, C. Chande, S. Chatterjee, S. Basuray, A highly sensitive, easy-and-rapidly-fabricable microfluidic electrochemical cell with an enhanced three-dimensional electric field, Anal. Chim. Acta 1232 (2022) 340488.
- [8] I. Miranda, A. Souza, P. Sousa, J. Ribeiro, E.M. Castanheira, R. Lima, et al., Properties and applications of PDMS for biomedical engineering: a review, J. Funct. Biomater. 13 (2021) 2.
- [9] K.T.L. Trinh, D.A. Thai, W.R. Chae, N.Y. Lee, Rapid fabrication of poly (methyl methacrylate) devices for lab-on-a-chip applications using acetic acid and UV treatment, ACS Omega 5 (2020) 17396–17404.
- [10] A. Liga, J.A. Morton, M. Kersaudy-Kerhoas, Safe and cost-effective rapid-prototyping of multilayer PMMA microfluidic devices, Microfluid. Nanofluidics 20 (20) (2016) 1
- [11] D. Ogończyk, P. Jankowski, P. Garstecki, A method for simultaneous polishing and hydrophobization of polycarbonate for microfluidic applications, Polymers 12 (2020) 2400
- [12] J. Li, C. Liang, H. Zhang, C. Liu, Reliable and high quality adhesive bonding for microfluidic devices, Micro Nano Lett. 12 (2017) 90–94.
- [13] M.T. Koesdjojo, S. Pengpumkiat, Y. Wu, A. Boonloed, D. Huynh, T.P. Remcho, et al., Cost effective paper-based colorimetric microfluidic devices and mobile phone camera readers for the classroom, J. Chem. Educ. 92 (2015) 737–741.
- [14] Y.S. Kim, Y. Yang, C.S. Henry, Laminated and infused Parafilm®-paper for paper-based analytical devices, Sens. Actuators B: Chem. 255 (2018) 3654–3661.
- [15] S. Kasetsirikul, K. Clack, M.J. Shiddiky, N.-T. Nguyen, Rapid, simple and inexpensive fabrication of paper-based analytical devices by Parafilm® hot pressing, Micromachines 13 (2021) 48.
- [16] D.I. Walsh, D.S. Kong, S.K. Murthy, P.A. Carr, Enabling microfluidics: from clean rooms to makerspaces, Trends Biotechnol. 35 (2017) 383–392.
- [17] Y. Sameenoi, K. Koehler, J. Shapiro, K. Boonsong, Y. Sun, J. Collett Jr, et al., Microfluidic electrochemical sensor for on-line monitoring of aerosol oxidative activity, J. Am. Chem. Soc. 134 (2012) 10562–10568.
- [18] L. Zhu, X. Liu, J. Yang, Y. He, Y. Li, Application of multiplex microfluidic electrochemical sensors in monitoring hematological tumor biomarkers, Anal. Chem. 92 (2020) 11981–11986.
- [19] A. Martín, J. Kim, J.F. Kurniawan, J.R. Sempionatto, J.R. Moreto, G. Tang, et al., Epidermal microfluidic electrochemical detection system: Enhanced sweat sampling and metabolite detection. ACS Sens. 2 (2017) 1860–1868.
- [20] D.G. Rackus, M.H. Shamsi, A.R. Wheeler, Electrochemistry, biosensors and microfluidics: a convergence of fields, Chem. Soc. Rev. 44 (2015) 5320–5340.
- [21] X. Zhao, C. Hinchliffe, C. Johnston, P.J. Dobson, P.S. Grant, Spray deposition of polymer nanocomposite films for dielectric applications, Mater. Sci. Eng.: B 151 (2008) 140–145.
- [22] N. Na, M. Zhao, S. Zhang, C. Yang, X. Zhang, Development of a dielectric barrier discharge ion source for ambient mass spectrometry, J. Am. Soc. Mass Spectrom. 18 (2007) 1859–1862.
- [23] H. Ervasti, T. Jarvinen, O. Pitkanen, É. Bozó, J. Hiitola-Keinanen, O.-H. Huttunen, et al., Inkjet-deposited single-wall carbon nanotube micropatterns on stretchable PDMS-Ag substrate-electrode structures for piezoresistive strain sensing, ACS Appl. Mater. Interfaces 13 (2021) 27284–27294.
- [24] L. Bai, Y. Lim, Y. He, Q. Xiong, S. Hou, J. Zhang, et al., Hierarchical disordered colloidal thin films with duplex optical elements for advanced anti-counterfeiting coding, Adv. Opt. Mater. 8 (2020) 2001378.

- [25] J. Yuan, G. Sahni, Y.-C. Toh, Stencil micropatterning for spatial control of human pluripotent stem cell fate heterogeneity, Stem Cell Heterog.: Methods Protoc. (2016) 171–181.
- [26] E. Rafatmah, B. Hemmateenejad, Fabrication of the first disposable three-dimensional paper-based concentration cell as ammonia sensor with a new method for paper hydrophobization by laser patterned Parafilm®, Electroanalysis 31 (2019) 632–638.
- [27] S.K. Tiwari, S. Bhat, K.K. Mahato, Design and fabrication of low-cost microfluidic channel for biomedical application, Sci. Rep. 10 (2020) 9215.
- [28] S. Kaaliveetil, J. Yang, S. Alssaidy, Z. Li, Y.-H. Cheng, N.H. Menon, et al., Microfluidic gas sensors: detection principle and applications, Micromachines 13 (2022) 1716.
- [29] Y. Lu, Z. Shi, L. Yu, C.M. Li, Fast prototyping of a customized microfluidic device in a non-clean-room setting by cutting and laminating Parafilm®, RSC Adv. 6 (2016) 85468–85472
- [30] S.Z. Akash, F.Y. Lucky, M. Hossain, A.K. Bepari, G.S. Rahman, H.M. Reza, et al., Remote temperature-responsive parafilm dermal patch for on-demand topical drug delivery, Micromachines 12 (2021) 975.
- [31] L. Zhang, L. Sun, M. Hou, Z. Xu, Y. Kang, P. Xue, A paper-based photothermal array using Parafilm to analyze hyperthermia response of tumour cells under local gradient temperature, Biomed. Micro 20 (2018) 1–10.
- [32] A. Lamberti, A. Sacco, S. Bianco, E. Giuri, M. Quaglio, A. Chiodoni, et al., Microfluidic sealing and housing system for innovative dye-sensitized solar cell architecture, Microelectron. Eng. 88 (2011) 2308–2310.
- [33] C. Liu, J.A. Thompson, H.H. Bau, A membrane-based, high-efficiency, microfluidic debubbler, Lab a Chip 11 (2011) 1688–1693.
- [34] B. Qiu, X. Chen, F. Xu, D. Wu, Y. Zhou, W. Tu, et al., Nanofiber self-consistent additive manufacturing process for 3D microfluidics, Microsyst. Nanoeng. 8 (2022) 102.

Zhenglong Li – Ph.D. Student at the Department of Chemical and Materials Engineering, Newark, New Jersey 07102, United States

Niranjan Haridas – Ph.D. Student at the Department of Chemical and Materials Engineering, Newark, New Jersey 07102, United States

Sreerag Kaaliveetil – Ph.D. Student at the Department of Chemical and Materials Engineering, Newark, New Jersey 07102, United States

Yu-Hsuan Cheng – Ph.D. Student at the Department of Chemical and Materials Engineering, Newark, New Jersey 07102, United States

Charmi Chande – Postdoctor at the Department of Chemical and Materials Engineering, Newark, New Jersey 07102, United States

Veronica Perez – Master Student at the Department of Biomedical Engineering, Newark, New Jersey 07102, United States

Amir K. Miri – Assistant Professor at the Department of Biomedical Engineering, Newark, New Jersey 07102, United States